Available online at www.sciencedirect.com
ScienceDirect
International Journal of Fatigue 29 (2007) 1100–1114
International Journal of Fatigue
www.elsevier.com/locate/ijfatigue

Online fatigue damage monitoring by ultrasonic measurements: A symbolic dynamics approach ☆

Shalabh Gupta, Asok Ray *, Eric Keller

Mechanical Engineering Department, The Pennsylvania State University, 329 Reber Building, University Park, PA 16802, United States

Received 1 December 2005; received in revised form 12 August 2006; accepted 10 September 2006
Available online 31 October 2006

Abstract

The paper presents an analytical tool for early detection and online monitoring of fatigue damage in polycrystalline alloys that are commonly used in mechanical structures of human-engineered complex systems. Real-time fatigue damage monitoring algorithms rely on time series analysis of ultrasonic signals that are sensitive to micro-structural changes occurring inside the material during the early stages of fatigue damage; the core concept of signal analysis is built upon the principles of *Symbolic Dynamics*, *Statistical Pattern Recognition* and *Information Theory*. The analytical tool of statistical pattern analysis has been experimentally validated on a special-purpose test apparatus that is equipped with ultrasonic flaw detection sensors and a travelling optical microscope. The paper reports fatigue damage monitoring of 7075-T6 alloy specimens, where the experiments have been conducted under load-controlled constant amplitude sinusoidal loadings for low-cycle and high-cycle fatigue.

Keywords: Symbolic time series analysis; Anomaly detection; Fatigue damage

1. Introduction

Prediction of structural damage and quantification of structural integrity are critical for safe and reliable operation of human-engineered complex systems. Fatigue damage is one of the most commonly encountered sources of structural degradation during both nominal and off-nominal operations of such systems [1]. Therefore, it is necessary to develop diagnosis and prognosis capabilities for reliable and safe operation of the system and for enhanced availability of its service life. Many model-based techniques have been reported in literature for structural health monitoring and life prediction [2–5]. Apparently, no existing model, solely based on the fundamental principles of molecular physics [6], can adequately capture the dynamical behavior of fatigue damage at the grain level. In general, model-based approaches are critically dependent on initial defects in the material micro-structure, which may randomly form crack nucleation sites and are difficult to model [1,7]. Small deviations in initial conditions and critical parameters may produce large bifurcations in the expected dynamical behavior of fatigue damage [8]. In addition, fluctuations in usage patterns (e.g., random overloads) and environmental conditions (e.g., temperature and humidity) may adversely affect the service life of mechanical systems. As such, fatigue damage is described as a stochastic phenomenon that emphasizes the need for online monitoring using sensing devices which can provide useful and reliable estimates of the anomalies at an early stage [9].

Information-based fatigue damage monitoring using different sensors (e.g., acoustic emission, eddy currents and ultrasonic) has been proposed in recent literature [10–12]. The capabilities of electrochemical sensors [13] and thermal imaging techniques [14] have also been investigated for structural failure analysis. The traditional analysis methods

☆ This work has been supported in part by the US Army Research Laboratory and the US Army Research Office (ARO) under Grant No. DAAD19-01-1-0646.
* Corresponding author.
E-mail addresses: szg107@psu.edu (S. Gupta), axr2@psu.edu (A. Ray), eek105@psu.edu (E. Keller).

0142-1123/$ - see front matter © 2006 Elsevier Ltd. All rights reserved.
doi:10.1016/j.ijfatigue.2006.09.011

Nomenclature

D	window length on a symbolic sequence	σ	a symbol on a symbolic sequence
n	number of states of the finite state machine	π^{jk}	transition probability from state q_j to q_k
$\mathbf{p}^k$	state probability vector at time epoch t_k	Π^k	state transition matrix at time epoch t_k
$P(\bullet)$	Probability of the event $\bullet$	ψ^k	anomaly measure computed at time epoch t_k
q_j	jth state of the finite state machine	Φ_j	jth block of the partition of the phase space
Q	set of all states of the finite state machine	Ω	phase space of a dynamical system
S	dynamical systems entropy of the symbol sequence	Σ	alphabet set
		$\lvert\Sigma\rvert$	size of the alphabet set
t_k	slow time epoch		

using acoustic emission technique are used to correlate the signal parameters (such as the acoustic emission counts, the peak amplitudes and the energy) with the defect formation mechanisms and to provide a quantified estimate of faults. Acoustic emission technique has been investigated by several researchers for its sensitivity to the activities occurring inside the material micro-structure for early detection of fatigue and fracture failures [15–19]. However, the major drawback of acoustic emission technique is poor performance in noisy environments where signal–noise separation becomes a difficult task.

The eddy current technique is based on the principles of electromagnetic induction. When a source of alternating current is supplied to a conductor, a magnetic field develops, which induces eddy currents in the material. The presence of faults in the material affect the eddy current flow patterns, which can be detected for prediction and estimation of the structural damage [20–22]. The advantages of eddy current inspection technique include sensitivity to small cracks and other defects, portability of sensor equipment, minimum part preparation, and non-contact evaluation. However, the limitations of the eddy current inspection technique are the depth of penetration and it can be used to detect only surface and near surface defects. Furthermore, only conductive materials can be inspected.

Ultrasonic sensors function by emitting high-frequency ultrasonic pulses that travel through the specimen and are received by the transducers at the other end. As with the propagation of any wave, it is possible that discontinuities in the propagation media will cause additive and destructive interference. Since material characteristics (e.g., voids, dislocations and short cracks) influence the ultrasonic impedance, a small fault in the specimen is likely to change the signature of the signal at the receiver end [23,24,9,25,26]. Therefore, the ultrasonic signals can be used to capture some of the minute details and small changes during the early stages of fatigue damage, which may not be possible to detect by an optical microscope [9]. Moreover, ultrasonic sensing is applicable to real-time applications and the sensing probes can be easily installed at the critical sites. Ultrasonic sensing is also robust to noisy environments since the externally excited waves are of very high frequency and they do not interfere with small disturbances. As such, this paper explores the ultrasonic sensing technique to examine small micro-structural changes during early stages of fatigue damage evolution.

The above discussions evince the fact that time series analysis of sensor data is essential for real-time detection and monitoring of fatigue damage. From this perspective, the paper presents symbolic time series analysis (STSA) [27] of ultrasonic sensor signals for early detection of evolving anomalies. The STSA method is an information-theoretic pattern identification tool that is built upon a fixed-structure, fixed-order Markov chain [28]; it has been validated by comparison with existing pattern recognition techniques such as Principal Component Analysis (PCA) and Artificial Neural Networks (ANN) [29,30]. A computer-controlled special purpose test apparatus, equipped with multiple sensing devices (e.g., ultrasonics and optical microscope) for damage analysis, has been used to experimentally validate the STSA method of fatigue damage detection. Experiments have been conducted under different loading conditions on 7075-T6 aluminum alloy specimens.

The paper is organized in seven sections including the present section. Section 2 presents an overview of anomaly detection methodology using a two-time-scale approach. Section 3 describes the underlying concepts and essential features of symbolic time series analysis for anomaly detection. Section 4 provides a brief description of the fatigue damage test apparatus. Section 5 presents the experimental procedure and the application of STSA for fatigue damage monitoring. Section 6 presents the results and discussion on early detection of fatigue damage under different loading conditions. The paper is concluded in Section 7 along with recommendations for future research.

2. Methodology for fatigue damage monitoring

Traditional tools like S–N curves and Goodman diagrams are not effective for real-time damage prediction. This problem is circumvented by information-based diagnosis and prognosis tools that are capable of identifying damage patterns in real time from the statistical behavior of sensor (e.g., ultrasonic) data sequences. In this context,

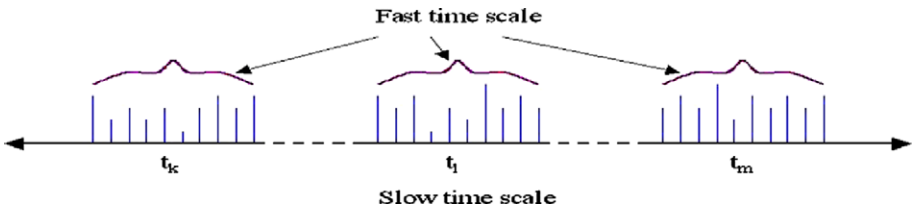

Fig. 1. Pictorial view of the two time scales: (1) *slow time scale* where anomalies evolve and (2) *fast time scale* where data acquisition is done.

fatigue damage monitoring is formulated as a two-time-scale problem. The sampling frequency for data acquisition is required to be several orders of magnitude faster than the time period of damage evolution. Fatigue damage monitoring is a two-time-scale problem as delineated below:

- The *fast time scale* is related to the response time of machinery operation. Over the span of a given time series data sequence, the structural dynamic behavioral statistics of the system are assumed to remain invariant, i.e., the process is assumed to have statistically stationary dynamics at the fast time scale.
- The *slow time scale* is related to the time span over which the process may exhibit non-stationary dynamics due to (possible) evolution of anomalies. Thus, an observable non-stationary behavior can be associated with anomalies evolving at a slow time scale.

A pictorial view of the two time scales is presented in Fig. 1. In general, a long time span in the fast time scale is a tiny (i.e., several orders of magnitude smaller) interval in the slow time scale. For example, evolution of fatigue damage in structural materials (causing a detectable change in the dynamics of the system) occurs on the slow time scale (possibly in the order of months or years); fatigue damage behavior is essentially invariant on the fast time scale (approximately in the order of seconds or minutes). Nevertheless, the notion of fast and slow time scales is dependent on the specific application, loading conditions and operating environment. As such, from the perspective of fatigue monitoring, sensor data acquisition is done on the fast time scale at different slow time epochs separated by fixed intervals on the slow time scale. Specifically, the objective of this paper is to demonstrate real-time monitoring of fatigue damage by detecting small changes in the statistical patterns of the ultrasonic sequences using the STSA approach.

3. Symbolic time series analysis for anomaly detection

This section presents the underlying concepts and essential features of symbolic time series analysis [27] for anomaly detection in complex dynamical systems [28]. While the details are reported in previous publications [28,29,31]; a brief review of this method is presented here for completeness and clarity of the paper. The principle of symbolic dynamics is based on the transformation of a data sequence (e.g., time series data) to a symbol sequence by partitioning a compact region Ω of the phase space, over which the trajectory evolves, into finitely many discrete blocks as shown in Fig. 2. Let $\{\Phi_1, \Phi_2, \ldots, \Phi_m\}$ be a partitioning of Ω, such that it is exhaustive and mutually exclusive set, i.e.,

$$\bigcup_{j=1}^{m} \Phi_j = \Omega \quad \text{and} \quad \Phi_j \bigcap \Phi_k = \emptyset \quad \forall j \neq k. \tag{1}$$

Each block Φ_j is labelled as the symbol $\sigma_j \epsilon \Sigma$, where the symbol set Σ is called the *alphabet set* consisting of m different symbols (i.e., $m = |\Sigma|$). As the system evolves in time, it travels through various blocks in its phase space and the corresponding symbol $\sigma_j \epsilon \Sigma$ is assigned to it, thus converting a data sequence to a symbol sequence $\ldots \sigma_{i_1} \sigma_{i_2} \ldots \sigma_{i_k} \ldots$ [32,33]. Fig. 2 exemplifies the partitioning of the phase space where each block is assigned a particular symbol such that a symbol sequence is generated from the phase space at a given slow time epoch. Once the symbol sequence is obtained, the next step is construction of a finite state machine [34]. These steps are explained in details in the following subsections.

3.1. Wavelet space partitioning

A crucial step in symbolic time series analysis is partitioning of the phase space for symbol sequence generation [27]. Several partitioning techniques have been reported in literature for symbol generation [35–37], primarily based on symbolic false neighbors. These techniques rely on partitioning the phase space and may become cumbersome and extremely computation-intensive if the dimension of the phase space is large. Moreover, if the time series data is noise-corrupted, then the symbolic false neighbors would rapidly grow in number and require a large symbol alphabet to capture the pertinent information on the system dynamics. Therefore, symbolic sequences as representations of the system dynamics should be generated by alternative methods because phase-space partitioning might prove to be a difficult task in the case of high-dimensions and presence of noise. The wavelet transform [38] largely alleviates these shortcomings and is particularly effective with noisy data from high-dimensional dynamical systems.

This paper has adopted a wavelet-based partitioning approach [28,31] for construction of symbol sequences from the time series data. In this method, the time series data are first converted by wavelet transform, where wavelet coefficients are generated at different scales and time shifts. The graphs of wavelet coefficients versus scale, at

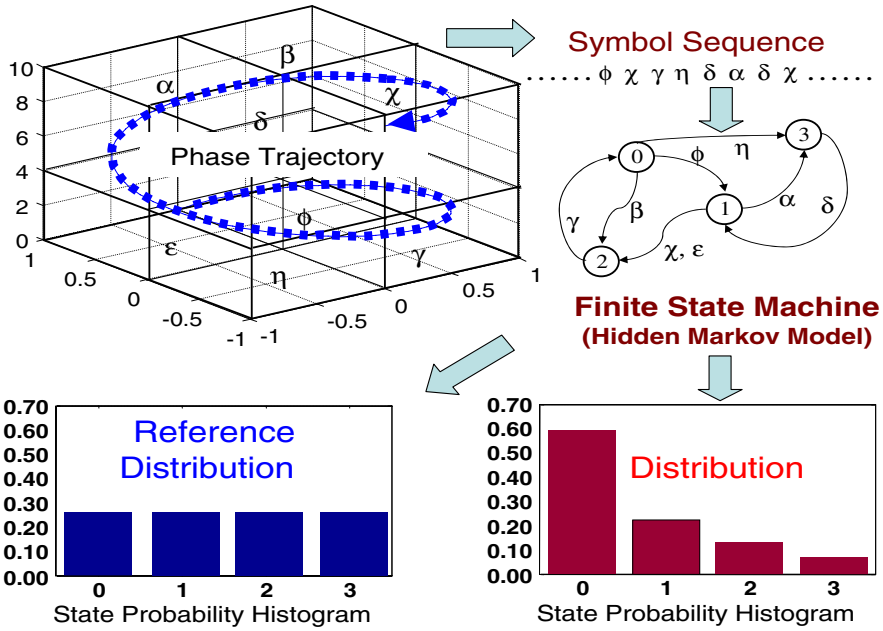

Fig. 2. STSA-based pattern identification.

selected time shifts, are stacked starting with the smallest value of scale and ending with its largest value and then back from the largest value to the smallest value of the scale at the next instant of time shift. The arrangement of the resulting *scale series* data in the wavelet space is similar to that of the time series data in the phase space. The wavelet space is partitioned with alphabet size $|\Sigma|$ into segments of coefficients on the ordinate separated by horizontal lines such that the regions with more information are partitioned finer and those with sparse information are partitioned coarser. This is achieved by maximizing the Shannon entropy [39], which is defined as

$$S = -\sum_{i=1}^{|\Sigma|} p_i \log(p_i), \tag{2}$$

where p_i is the probability of the ith state and summation is taken over all possible states. Uniform probability distribution of states is a consequence of maximum entropy that makes the partition coarser in regions of low-data density and finer in regions of high-data density.

3.2. State machine construction

The partitioning as described in the previous section is performed at time epoch t_0 of the nominal condition that is chosen to be a healthy condition having zero anomaly measure. A finite state machine [34] is then constructed, where the states of the machine are defined corresponding to a given *alphabet* Σ and window length D. The alphabet size $|\Sigma|$ is the total number of partitions while the window length D is the length of consecutive symbol words forming the states of the machine [28]. The states of the machine are chosen as all possible words of length D from the symbol sequence, thereby making the number n of states to be equal to the total permutations of the alphabet symbols within words of length D, (i.e., $n \leqslant |\Sigma|^D$; some of which may be forbidden with zero probability of occurrence). For example, if $\Sigma = \{0, 1\}$, i.e., $|\Sigma| = 2$ and $D = 2$, then the number of states is $n \leqslant |\Sigma|^D = 4$; and the possible states are $Q = \{00, 01, 10, 11\}$.

The choice of $|\Sigma|$ and D depends on specific experiments, noise level and also the available computation power. A large *alphabet* may be noise-sensitive while a small alphabet could miss the details of signal dynamics. Similarly, a high-value of D is extremely sensitive to small signal distortions but would lead to a large number of states requiring more computation power. Using the symbol sequence generated from the time series data, the state machine is constructed on the principle of sliding block codes [32] as explained below. The window of length D on the symbol sequence $\ldots \sigma_{i_1}\sigma_{i_2}\ldots\sigma_{i_k}\ldots$ is shifted to the right by one symbol, such that it retains the last $(D-1)$ symbols of the previous state and appends it with the new symbol σ_{i_ℓ} at the end. The symbolic permutation in the current window gives rise to a new state. The machine constructed in this fashion is called D-Markov machine [28] because of its Markov properties.

Definition 3.1. A symbolic stationary process is called D-Markov if the probability of the next symbol depends only on the previous D symbols, i.e., $P(\sigma_{i_0}/\sigma_{i_{-1}}\ldots\sigma_{i_{-D}}\sigma_{i_{-D-1}}\ldots) = P(\sigma_{i_0}/\sigma_{i_{-1}}\ldots\sigma_{i_{-D}})$.

The finite state machine constructed above has D-Markov properties because the probability of occurrence of symbol σ_{i_ℓ} on a particular state depends only on the

configuration of that state, i.e., the previous D symbols. Once the partitioning *alphabet* Σ and word length D are determined at the nominal condition (time epoch t_0), they are kept constant for all (slow time) epochs $\{t_1, t_2, \ldots, t_k \ldots\}$, i.e., the structure of the machine is fixed at the nominal condition. That is, the partitioning and the state machine structure generated at the nominal condition serve as the reference frame for data analysis at subsequent time epochs. For $D = 1$, the set of states bears an equivalence relation to the alphabet Σ of symbols [40]. The states of the machine are marked with the corresponding symbolic word permutation and the edges joining the states indicate the occurrence of an event σ_{i_ℓ}. The occurrence of an event at a state may keep the machine in the same state or move it to a new state. The language of the machine is usually incomplete in the sense that all states might not be reachable from a given state.

Definition 3.2. The probability of transitions from state q_j to state q_k belonging to the set Q of states under a transition δ: $Q \times \Sigma \to Q$ is defined as

$$\pi_{jk} = P(\sigma \in \Sigma | \delta(q_j, \sigma) \to q_k); \sum_k \pi_{jk} = 1. \tag{3}$$

Thus, for a D-Markov machine, the irreducible stochastic matrix $\Pi \equiv [\pi_{ij}]$ describes all transition probabilities between states such that it has at most $|\Sigma|^{D+1}$ nonzero entries. The left eigenvector $\mathbf{p}$ corresponding to the unit eigenvalue of Π is the state probability vector under the (fast time scale) stationary condition of the dynamical system [28]. On a given symbol sequence $\ldots \sigma_{i_1} \sigma_{i_2} \ldots \sigma_{i_l} \ldots$ generated from the time series data collected at slow time epoch t_k, a window of length (D) is moved by keeping a count of occurrences of word sequences $\sigma_{i_1} \ldots \sigma_{i_D} \sigma_{i_{D+1}}$ and $\sigma_{i_1} \ldots \sigma_{i_D}$ which are respectively denoted by $N(\sigma_{i_1} \ldots \sigma_{i_D} \sigma_{i_{D+1}})$ and $N(\sigma_{i_1} \ldots \sigma_{i_D})$. Note that if $N(\sigma_{i_1} \ldots \sigma_{i_D}) = 0$, then the state $q \equiv \sigma_{i_1} \ldots \sigma_{i_D} \in Q$ has zero probability of occurrence. For $N(\sigma_{i_1} \ldots \sigma_{i_D}) \neq 0$, the transitions probabilities are then obtained by these frequency counts as follows:

$$\pi_{jk} \equiv P[q_k | q_j] = \frac{P[q_k, q_j]}{P[q_j]} = \frac{P(\sigma_{i_1} \ldots \sigma_{i_D} \sigma)}{P(\sigma_{i_1} \ldots \sigma_{i_D})} \Rightarrow \pi_{jk} \approx \frac{N(\sigma_{i_1} \ldots \sigma_{i_D} \sigma)}{N(\sigma_{i_1} \ldots \sigma_{i_D})}, \tag{4}$$

where the corresponding states are denoted by $q_j \equiv \sigma_{i_1} \sigma_{i_2} \ldots \sigma_{i_D}$ and $q_k \equiv \sigma_{i_2} \ldots \sigma_{i_D} \sigma$. The time series data under the nominal condition (set as a benchmark) generates the *state transition matrix* Π^0 that, in turn, is used to obtain the *state probability vector* $\mathbf{p}^0$ whose elements are the stationary probabilities of the state vector, where $\mathbf{p}^0$ is the left eigenvector of Π^0 corresponding to the (unique) unit eigenvalue. Subsequently, state probability vectors $\mathbf{p}^1, \mathbf{p}^2, \ldots, \mathbf{p}^k, \ldots$ are obtained at slow time epochs $t_1, t_2, \ldots, t_k, \ldots$ based on the respective time series data. Machine structure and partitioning should be the same at all slow time epochs.

3.3. Pattern identification procedure

Behavioral pattern changes are quantified as deviations from the nominal behavior (i.e., the probability distribution at the nominal condition). The resulting anomalies (i.e., deviations of the evolving patterns from the nominal pattern) are characterized by a scalar-valued function, called *Anomaly Measure* ψ that is quasi-static in the fast time scale and is monotonically non-decreasing in the slow time scale. The state probability vector at any time instant corresponds to a singleton point on the unity-radius hypersphere. During fatigue damage evolution, the tip of the probability vector moves along a path on the surface of this hypersphere. The initial starting point of the path is the probability vector with uniform distribution obtained with maximum entropy partitioning (see Section 3.1). As the damage progresses, the probability distribution changes; eventually when a very large crack is formed, complete attenuation of the ultrasonic signal occurs and consequently the tip of the probability vector reaches a point where all states have zero probabilities of occurrence except one which has a probability one (i.e., a delta-distribution); this state corresponds to the partition region where all data points are clustered due to complete attenuation of the signal.

In the context of fatigue damage, the anomaly measure is formulated on the following assumptions.

- *Assumption* #1: The damage evolution is an irreversible process (i.e., with zero probability of self healing) and implies the following conditions.

$$\psi^k \geqslant 0; \ \psi^{k+\ell} - \psi^k \geqslant 0 \quad \forall \ell \geqslant 0 \quad \forall k. \tag{5}$$

- *Assumption* #2: The damage accumulation between two time epochs is a path function, i.e., dependent on the path traversed to reach the target state from the initial state.

In the context of fatigue damage in polycrystalline alloys at room temperature, the crack length is traditionally defined by a straight line joining the starting point to the tip of the crack but, in reality, the actual crack follows a complicated path (possibly fractal in ductile materials). In fact, at the initial stages of fatigue damage, there can be multiple short cracks oriented in different directions. Therefore, crack length alone does not provide complete information on fatigue damage evolution. Since ultrasonic signals are highly sensitive to small micro-structural changes, signal distortion is a good index of anomaly growth. The tip of the probability vector, obtained through symbolic time series analysis, moves along a curved path on the surface of the unity-radius hypersphere between the initial point $\mathbf{p}^0$ (i.e., uniform distribution obtained under maximum entropy partitioning) and the final point at very large crack formation $\mathbf{p}^f$ (i.e., δ-distribution due to complete attenuation of the signal). The phenomenon such as piling up of dislocations, strain hardening or reflec-

tions from multiple crack surfaces affect the ultrasonic signals in a variety of ways. An increase of the ultrasonic amplitude is also observed during very early stages of fatigue damage due to hardening of the material. On the other hand, ultrasonic signals attenuate sharply at the crack propagation stage upon development of a large crack.

As such, distortion of ultrasonic signals at a single time epoch may not uniquely determine the state of fatigue damage. The rationale is that two signals may exhibit similar characteristics but, in terms of actual incurred damage, the states are entirely different. Consequently, fatigue damage is a path function instead of being a state function. This assessment is consistent with assumption #1 implying that the damage evolution is irreversible. That is, at two different time epochs, the damage cannot be identical unless the net damage increment is zero. Consequently, by assumption #2, the anomaly measure should follow the traversed path of the probability vector, not the straight line joining the end points (i.e., the tips of the probability vectors).

The anomaly measure, based on the path between the nominal state to the completely damaged state, can be different even for identical test samples and under the same loading conditions because of the stochastic nature of fatigue phenomena. As such, analysis of a stochastic data set collected under identical experimental conditions is essential for identification of variations in different data sets. The following distance function is derived between probability vectors at two time epochs:

$$d(\mathbf{p}^k, \mathbf{p}^l) \equiv \sqrt{(\mathbf{p}^k - \mathbf{p}^l)^{\mathrm{T}}(\mathbf{p}^k - \mathbf{p}^l)}. \tag{6}$$

The algorithm for computation of the anomaly measure ψ compensates for spurious measurement and computation noise in terms of the sup norm which is defined as $\|\mathbf{e}\|_\infty \equiv \max(|e_1|, \ldots, |e_m|)$ of the error in the probability vector (i.e., the maximum error in the elements of the probability vector). The algorithm is presented below.

(i) $\psi^0 = 0$; $\delta\psi^1 = 0$; $\widetilde{\mathbf{p}} = \mathbf{p}^0$; $k = 1$;
(ii) if $\|\mathbf{p}^k - \widetilde{\mathbf{p}}\|_\infty > \epsilon$ then $\delta\psi^k = d(\mathbf{p}^k, \widetilde{\mathbf{p}})$ and $\widetilde{\mathbf{p}} \leftarrow \mathbf{p}^k$;
(iii) $\psi^k = \psi^{k-1} + \delta\psi^k$;
(iv) $k \leftarrow k + 1$; $\delta\psi^k = 0$; go to step (ii).

The real positive parameter ϵ, is associated with the robustness of the measure against measurement and computation noise and is identified by performing an experiment with a sample with no notch. Since there is no notch there is practically no stress augmentation and relatively no fatigue damage. As such, the parameter ϵ is estimated as

$$\epsilon \approx \max_{l \in \{1,\ldots,N\}} (\|\mathbf{p}^{l+1} - \mathbf{p}^l\|_\infty) \tag{7}$$

from N consecutive observations with $N \gg 1$.

The algorithm works in the following fashion: the reference point $\widetilde{\mathbf{p}}$ is initialized to the starting point $\mathbf{p}^0$ and anomaly measure ψ^0 is set to 0. At any slow time epoch t_k if the state probability vector moves such that the distance travelled in any particular direction (i.e., the sup norm $\|\bullet\|_\infty$) is greater than ϵ as specified in step (ii), then the anomaly measure is incremented by $\delta\psi^k = d(\mathbf{p}^k, \widetilde{\mathbf{p}})$ and the reference point is shifted to the current point $\mathbf{p}^k$. The procedure is repeated at all slow time epochs. As such, the total path travelled by the tip of probability vector represents the deviation from the nominal condition and the associated damage.

3.4. Real-time implementation

Fatigue damage monitoring using STSA has been successfully implemented in real time. The nominal condition is chosen after the start of the experiment at time epoch t_0, when the system attains a steady state and is considered to be in a healthy condition. The function module for STSA is triggered at this point. The D-Markov machine states are fixed in advance using *a priori* determined values of the parameters: alphabet size $|\Sigma|$ and window length D. The tasks of wavelet space partitioning and D-Markov machine construction are performed based on the time series data at the slow time epoch t_0 (nominal condition). The state probability vector $\mathbf{p}^0$ at time epoch t_0 is stored for computation of anomaly measures at subsequent slow time epochs, $t_1, t_2, \ldots, t_k, \ldots$, which are chosen to be separated by uniform intervals of time in these experiments. The ultrasonic data files at time epochs $t_0, t_1, \ldots, t_k, \ldots$ are read by the STSA function module that calculates the anomaly measure values at these time epochs. The algorithm is computationally very fast (i.e., several orders of magnitude faster relative to slow time scale damage monitoring) and the evolution of anomaly measure is exhibited in real time. The plot is updated with the most recent value of anomaly measure at each (slow time) epoch. Thus, the STSA algorithm allows on-line health monitoring and is capable of issuing warnings of incipient failures well in advance.

3.5. Advantages of STSA

After having discussed the underlying principles and essential features of STSA, the major advantages of STSA for anomaly detection are listed below:

(a) *Robustness to measurement noise and spurious signals* [31] – The procedure of STSA is robust to measurement noise and spurious disturbances and it filters out the noise at different steps. First of all, coarse graining of the continuous data (i.e., partitioning into finite blocks) and generation of a symbol sequence eliminate small measurement noise [28]. Secondly, the wavelet transform also contributes in signal–noise separation of the raw time series data by proper choice of scales [31]. Finally, the state probabilities are generated by passing a long symbol sequence over the finite state machine, which further eliminates small (zero-mean) measurement noise.

(b) Adaptability to low-resolution sensing due to coarse graining in space partitions [28].
(c) Capability for early detection of anomalies because of sensitivity to signal distortion and real-time execution on commercially available inexpensive platforms [30,29].
(d) Applicability to networked communication systems due to the capability of data compression into low-dimensional pattern vectors.

3.6. Summary of STSA based anomaly detection

The symbolic time series analysis (STSA) procedure of anomaly detection is summarized below.

- Acquisition of time series data from appropriate sensor(s) at time epoch t_0 of the nominal condition, when the system is assumed to be in the healthy state (i.e., zero anomaly measure).
- Generation of the wavelet transform coefficients, obtained with an appropriate choice of the wavelet basis and scale range.
- Maximum entropy partitioning of the wavelet *scale series data* at the nominal condition (see Section 3.1); and generation of the corresponding symbol sequence. The partitioning is fixed for subsequent time epochs.
- Construction of the D-Markov machine states from the symbol alphabet size $|\Sigma|$ and the window length D, and generation of the state probability vector $\mathbf{p}^0$ at time epoch t_0.
- Generation of time series data sequences at subsequent slow time epochs, $t_1, t_2, \ldots, t_k, \ldots$, and their conversion to the wavelet domain to generate respective symbolic sequences based on the partitioning at time epoch t_0.
- Generation of the state probability vectors $\mathbf{p}^1, \mathbf{p}^2, \ldots, \mathbf{p}^k, \ldots$ at slow time epochs, $t_1, t_2, \ldots, t_k, \ldots$ from the respective symbolic sequences using the finite state machine constructed at time epoch t_0.
- Computation of scalar *Anomaly Measures* $\psi^1, \psi^2, \ldots, \psi^k, \ldots$ at time epochs, $t_1, t_2, \ldots, t_k, \ldots$

4. Experimental apparatus and sensors for damage detection

The experimental apparatus, shown in Fig. 3, is a special-purpose uniaxial fatigue testing machine, which is operated under load control or strain control at speeds up to 12.5 Hz; a detailed description of the apparatus and its design specifications are reported in [41]. The test specimens are subjected to tensile–tensile cyclic loading by a hydraulic cylinder under the regulation of computer-controlled electro-hydraulic servo-valves. The damage estimation and life prediction subsystem consists of data analysis software and the associated computer hardware. The process instrumentation and the control module of the fatigue test apparatus are briefly described below.

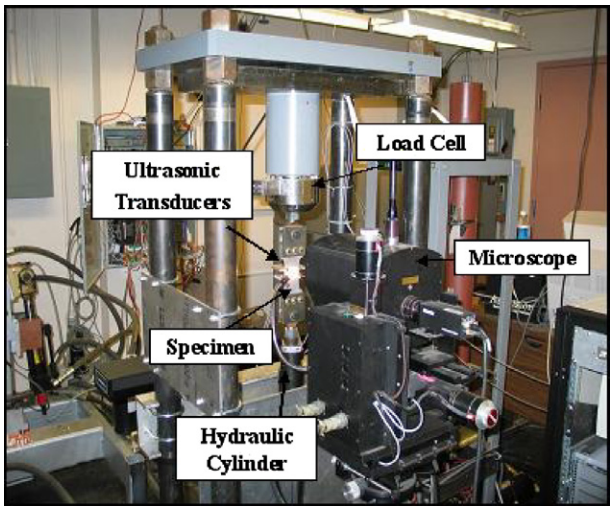

Fig. 3. Computer-instrumented apparatus for fatigue testing.

- *Closed loop servo-hydraulic unit and controller*: The instrumentation and control of the computer-controlled uniaxial fatigue test apparatus includes a load cell, an actuator, the hydraulic system, and the controller. The servo-hydraulic unit can provide either random loads or random strains to a specimen for both low-cycle and high-cycle fatigue tests at variable amplitudes and multiple frequencies. The control module is installed on a computer which is dedicated to machine operation. The controller runs the machine according to a schedule file which contains the loading profile and the number of load cycles. The real time data from the extensometer and load cell are supplied to the controller for operation under specified position and load limits.
- *Subsystem for data acquisition, signal processing, and engineering analysis*: In addition to the computer for controlling the load frame, a second computer is used for real-time image data collection from the microscope to monitor the growth of surface cracks. This computer controls the movement of the microscope to focus on the region of the crack tip. The instrumentation for ultrasonic flaw detection scheme is connected to a third computer. The ultrasonic data collected on this computer in real-time is then transferred at regular intervals to a fourth computer on which the STSA software is installed. This computer performs the real-time data analysis task. These laboratory computers are interconnected by a local dedicated network for data acquisition, data communications, and control.

Fig. 4 shows a typical 7075-T6 aluminum specimen used for testing in the fatigue damage test apparatus. The specimens used are 3 mm thick and 50 mm wide, and have a slot of 1.58 mm × 4.5 mm at the center. The central notch is made to increase the stress concentration factor that ensures crack initiation and propagation at the notch ends. The test specimens have been subjected to sinusoidal loading under tension–tension mode (i.e., with a constant posi-

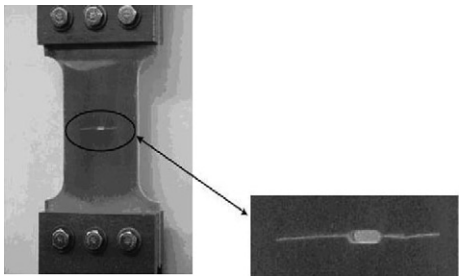

Fig. 4. Cracked specimen with a central notch.

tive offset) at a frequency of 12.5 Hz. The DC offset was provided in the load cycling to ensure that the specimen was always under tension. Since inclusions and flaws are randomly distributed across the material, small cracks appear at these defects and propagate and join at the machined surface of the notch even before microscopically visual cracks appear on the surface.

The test apparatus is equipped with two types of sensors that have been primarily used for damage detection:

(1) *Travelling optical microscope*: The travelling optical microscope, shown as part of the test apparatus in Fig. 3, provides direct measurements of the visible portion of a crack. The resolution of the optical microscope is about 2 μm at a working distance of 10–35 cm and the images are taken at a magnification of 75×. The growth of the crack is monitored continuously by the microscope which takes the images of the surface of the specimen at regular intervals. The microscope shifts from left to right side of the central notch and vice versa after every 200 cycles to track crack growth on both sides of the notch. In order to take pictures the controller slows down the machine to less than 5 Hz to get a better resolution of the images. The crack length can be calculated automatically by movement of the microscope from the respective notch end to the tip of the crack. The data acquisition software also allows for manual operation and image capture at the desired moment. Formation of very small cracks is difficult to detect and model due to large variability of material irregularities. This paper primarily focuses on analyzing ultrasonic data for more accurate characterization of the nature of small defects.

(2) *Ultrasonic flaw detector*: A piezoelectric transducer is used to inject ultrasonic waves in the specimen and an array of receiver transducers is placed on the other side of notch to measure the transmitted signal. In these experiments, an array of 2 receiver transducers was placed below the notch to detect faults on both left and right side of the notch. The ultrasonic waves produced were 5 MHz sine wave signals and they were emitted during a very short portion at the peak of every load cycle. Ultrasonic measurements were taken at stress levels that exceeded the crack opening stress and this causes maximum attenuation of the ultrasonic waves. Note that if crack closure occurs at low-loads, then an alternative method would be needed to detect anomalies. The sender and receiver ultrasonic transducers are placed on two positions, above and below the notch, so as to send the signal through the region of crack propagation and receive it on the other side, as seen in Fig. 5.

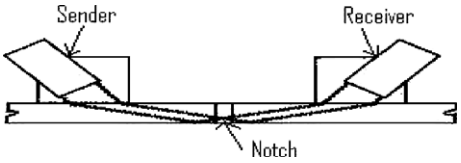

Fig. 5. Schematic of ultrasonic sensors on a test specimen.

As with the propagation of any wave, it is possible that discontinuities in the propagation media will cause additive and destructive interference. Since material characteristics (e.g., voids, dislocations and short cracks) influence ultrasonic impedance, a small fault in the specimen is likely to change the signature of the signal at the receiver end. The effect of these discontinuities in the material is to distort the transmitting ultrasonic waves. Since ultrasonic waves have a very small wavelength, very small faults can be detected. Therefore, the received signal can be used to capture minute details and small changes during the early stages of fatigue damage, which are not possible to detect by an optical microscope [9]. Prior to the appearance of a single large crack on the surface of the specimen as detected by the optical microscope, deformations (e.g., dislocations and short cracks) can cause detectable attenuation and/or distortion of the ultrasonic waves [25]. Recent literature has also shown nonlinear modelling approaches of the ultrasonic interference with the material micro-structures [42,43]. An elaborate description of the properties of ultrasonic waves in solid media is provided by Rose [44].

The advantages of using ultrasonic flaw detection over a microscope are the ease of installation at the desired damage site and detection of early anomalies before the onset of widespread fatigue crack propagation. It is observed that a crack always starts at the stress-concentrated region near the notch but the exact site of crack nucleation can be treated as a random event. An optical microscope is only capable of detecting cracks when they appear on the front surface of the specimen. Therefore, the study in this paper is based on analyzing the ultrasonic data for identification of fatigue damage in the small crack regime.

5. Experimentation and application of *STSA* for fatigue damage monitoring

The fatigue tests were conducted on center notched specimens with the objective of real-time continuous monitoring of fatigue damage growth on both sides of the notch. The tests were performed at 12.5 Hz frequency

under two different types of loading conditions: (a) *stress controlled low-cycle fatigue* and (b) *stress controlled high-cycle fatigue*. For low-cycle fatigue loading the specimens were subjected to a sinusoidal load where the maximum and minimum loads were kept constant at 92.5 MPa and 4.85 MPa. For high-cycle fatigue loading the maximum and minimum amplitudes were kept constant at 71 MPa and 4.85 MPa.

The optical images were collected automatically at every 200 cycles until a crack was detected on the specimen surface by the optical microscope. Subsequently, the images were taken at user command and the microscope was moved such that it always focused on the crack tip. A significant amount of micro-structural damage caused by multiple small cracks, dislocations and other defects occurs before a single large crack appears on the surface of the specimen when it is observed by the optical microscope [45]. This phenomenon causes distortion and attenuation of the ultrasonic signal at the receiver end. The crack propagation stage starts when this micro-structural damage eventually develops into a single large crack. Subsequently, the crack growth rate increases rapidly and when the crack is sufficiently large, complete attenuation of the transmitted ultrasonic signal occurs, as seen at the receiver end. After the crack appears on the surface, fatigue damage growth can be easily monitored by the microscope but the ultrasonics provide early warnings even during the crack initiation phase.

Ultrasonic waves with a frequency of 5 MHz were triggered at each peak of the sinusoidal load to obtain 100 data points in each cycle. Since the ultrasonic frequency is much higher than the load frequency, data acquisition was done for a very short interval in the time scale of load cycling. Therefore, it can be implied that ultrasonic data were collected at the peak of each sinusoidal load cycle, where the stress is maximum and the crack is open causing maximum attenuation of the ultrasonic waves. The slow time epochs were chosen to be 1000 load cycles (i.e., ~80 s) apart. At the onset of each slow time epoch, the ultrasonic data points were collected on the fast time scale of 100 cycles (i.e., ~8 s), which produced a string of 10,000 data points. It is assumed that during this fast time scale of 100 cycles, the system remained in a stationary condition and no major changes occurred in the fatigue damage behavior. This set of time series data collected in the manner described above at different slow time epochs was analyzed using the STSA method to calculate the anomaly measures at respective slow time epochs.

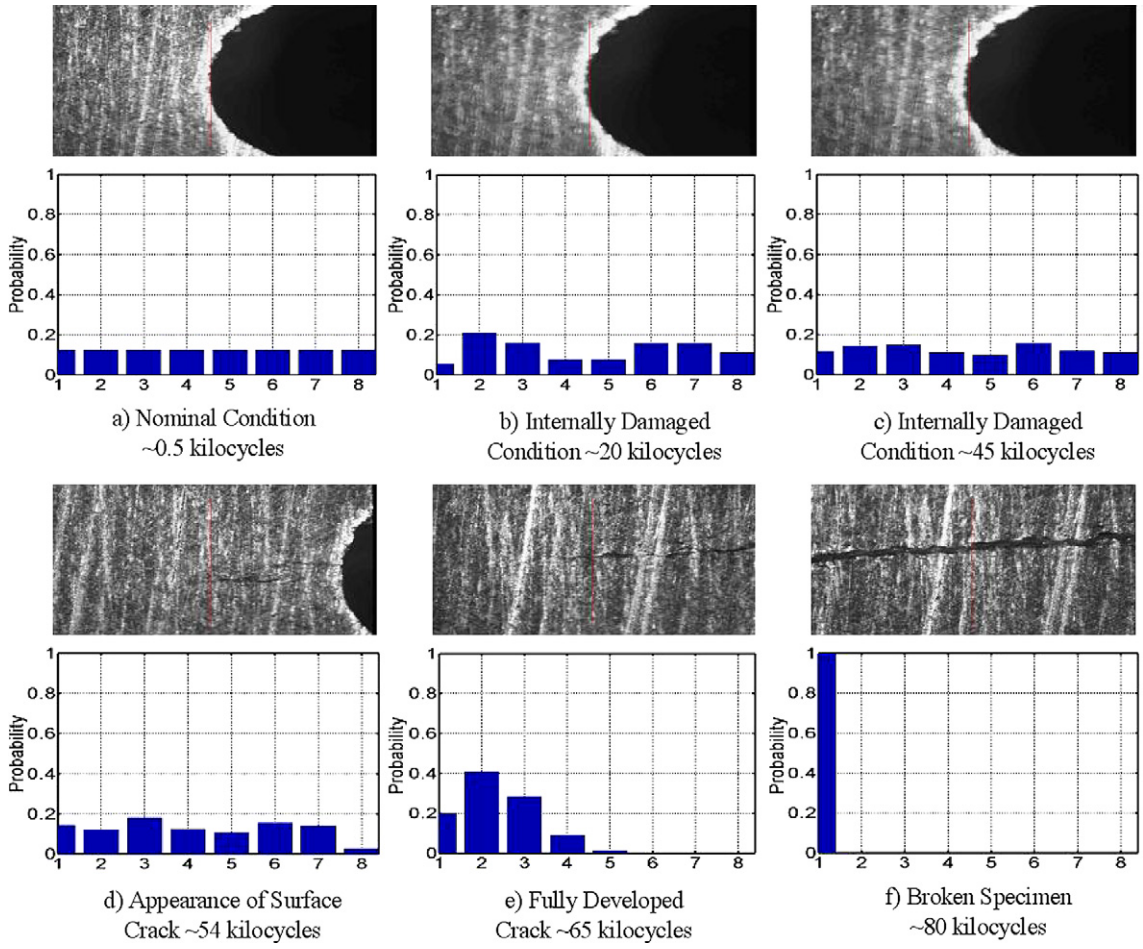

Fig. 6. Evolution of surface crack and probability distribution on left side of the notch under low cycle fatigue.

Following the STSA procedure for anomaly detection as described in Section 3, the alphabet size and depth have been chosen to be $|\Sigma| = 8$ and $D = 1$, respectively; consequently, the number of machine states is $|\Sigma|^D = 8$. The wavelet basis has been chosen to be 'gaus2' [46]. Absolute values of the wavelet scale series data have been used to generate the partition because of the symmetry of the data sets about their mean. With this selection, the STSA tool has been able to capture the anomalies significantly earlier than the optical microscope. Increasing the value of $|\Sigma|$ further did not improve the results and increasing the value of D created a large number of states of the finite state machine, many of them having very small or zero probabilities, and required a larger number of data points at each time epoch to stabilize the state probability vectors. The advantage of having a small number of states is fast computation on inexpensive processors and also robustness to noise. The wavelet basis, 'gaus2', provides better results than the wavelet bases of the Daubechies family [38] because the 'gaus2' wavelet base closely matches the shape of the sinusoidal ultrasonic signals.

The nominal condition at the slow time epoch t_0 was chosen to be ~0.5 kilocycles to ensure that the electro-hydraulic system of the test apparatus had come to a steady state and that no significant damage occurred till that point. This nominal condition was chosen as a benchmark where the specimen was assumed to be in a healthy state, and thus the anomaly measure was chosen to be zero. The anomalies at subsequent slow time epochs, $t_1, t_2, \ldots, t_k, \ldots$, were then calculated with respect to the nominal condition at t_0. It is emphasized that the anomaly measure is relative to the nominal condition which is fixed in advance and should not be confused with the actual damage at an absolute level. However, inferring fatigue damage from the observed anomaly measure is an inverse problem that is a topic of future research.

6. Experimental results and discussion

This section presents the results of symbolic time series analysis of the ultrasonic data generated by fatigue tests described in Section 5. In each of the six plate pairs from (a) to (f) in Figs. 6–9, the top plate displays the surface image of the test specimen, as seen by the optical microscope; and histograms of the state probability distribution in the bottom plates exhibit evolution of fatigue damage patterns at different slow time epochs. These patterns gradually change from uniform distribution (i.e., minimal

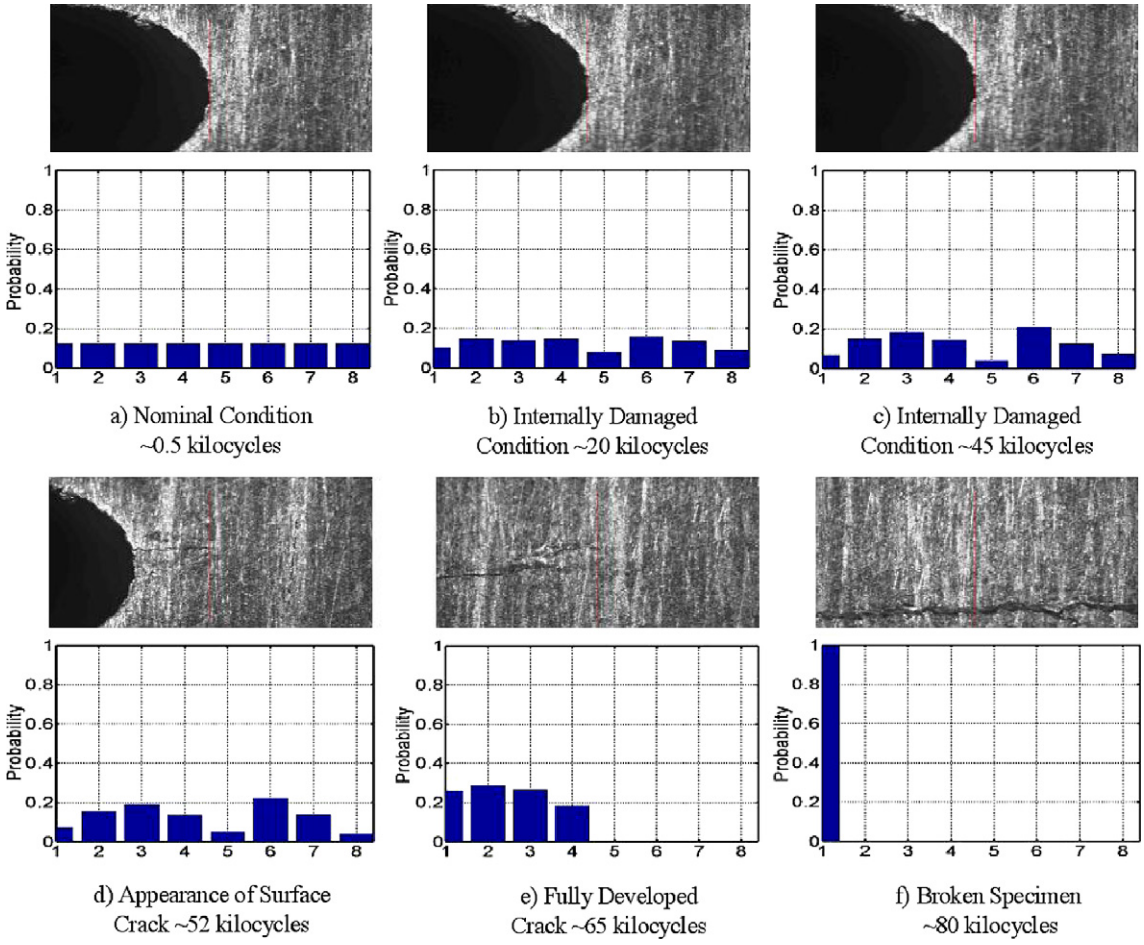

Fig. 7. Evolution of surface crack and probability distribution on right side of the notch under low cycle fatigue.

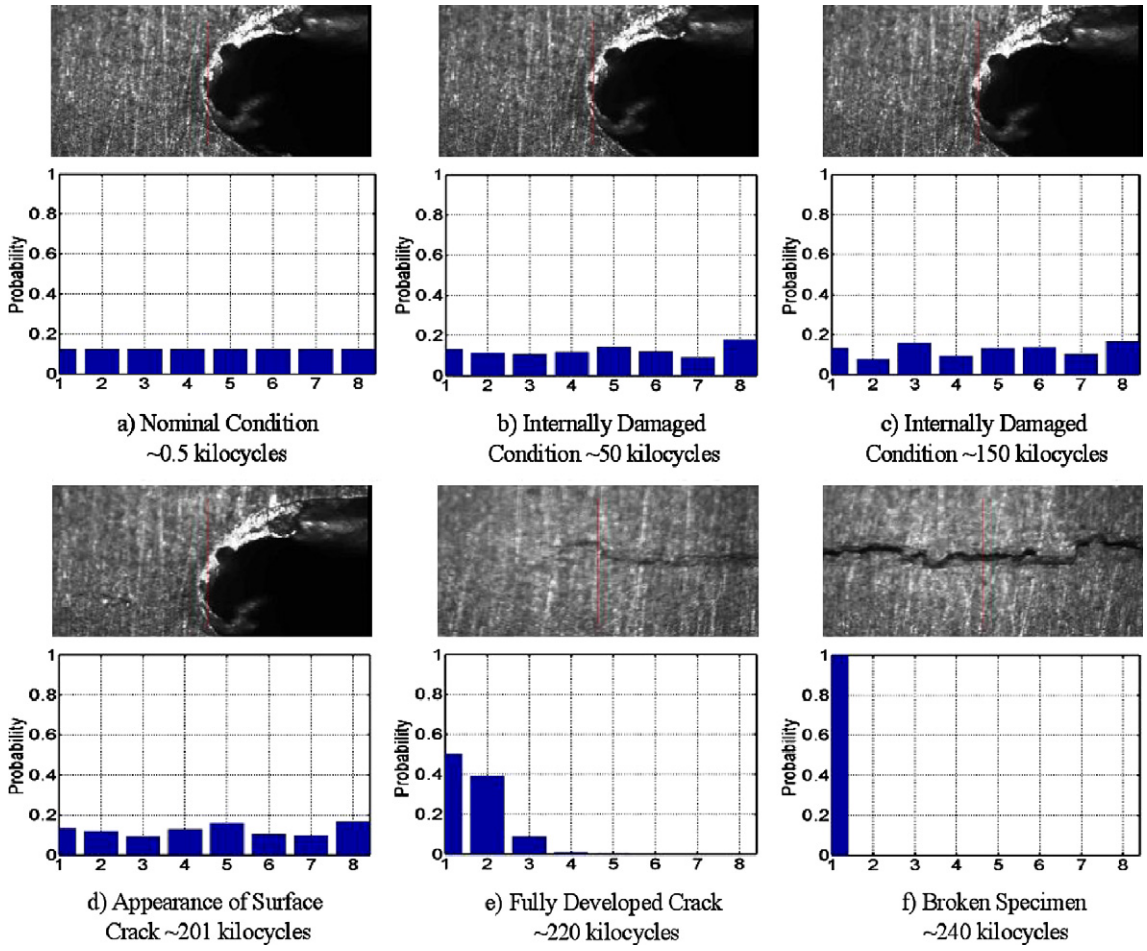

Fig. 8. Evolution of surface crack and probability distribution on left side of the notch under high-cycle fatigue.

information) to delta distribution (i.e., maximum information) in each figure.

The image in each of Figs. 6(a), 7(a), 8(a) and 9(a) shows the nominal condition at ~0.5 kilocycles when the anomaly measure is taken to be zero. This is considered to be the reference point with the available information on potential damage being minimal. This is reflected in the uniform distribution (i.e., maximum entropy or highest uncertainty) as seen from the histograms in the corresponding bottom plates.

The images in plate pairs (b) and (c) in Figs. 6–9 show the specimen surface before crack propagation. These images do not yet have any indication of surface crack although the corresponding bottom plates do exhibit deviations from the uniform probability distribution (see the bottom plate in plate pair (a) for comparison). This is an evidence that the analytically derived results, based on ultrasonic sensor data, produce relevant damage information during crack initiation; this information is not available from the corresponding optical images. For low-cycle fatigue in Figs. 6 and 7, the plate pairs (b) and (c) represent damage status at ~20 and ~45 kilocycles, respectively; and for high-cycle fatigue in Figs. 8 and 9, they represent damage status at ~50 and ~150 kilocycles, respectively. The deviations of these histograms from those at the nominal condition in plates (a) indicate that the probability vector has moved to another location on the surface of unity-radius hypersphere. The path depends on the interactions of the ultrasonic signals with the subsurface deformities.

The image in each of Figs. 6(d), 7(d), 8(d) and 9(d) exhibits the first noticeable appearance of a crack on the specimen surface, which is often deemed as the boundary of crack initiation and crack propagation phases; however, crack propagation might have started before the appearance of a surface crack. For low-cycle fatigue in Figs. 6 and 7, surface cracks have been detected by the microscope at ~54 and ~52 kilocycles on the left side and right side of the notch, respectively. Similarly, for high-cycle fatigue in Figs. 8 and 9, surface cracks have been detected at ~201 and ~215 kilocycles on left side and right side of the notch, respectively. The appearance of a large surface crack indicates that a significant portion of the crack or multiple small cracks might have already developed underneath the surface before they started spreading on the surface. However, further micro-structural analysis is need to confirm these findings. The histogram of probability distribution in the corresponding bottom plates show further

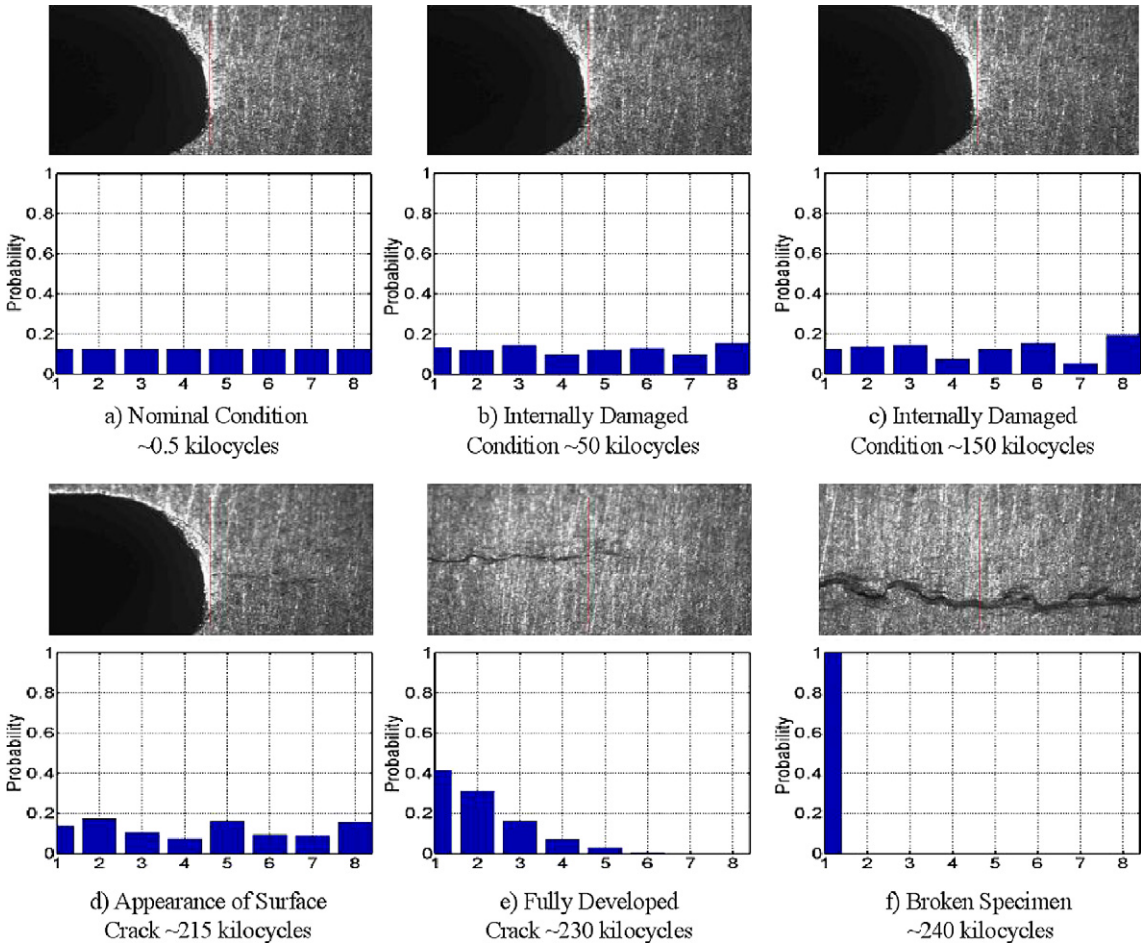

Fig. 9. Evolution of surface crack and probability distribution on right side of the notch under high-cycle fatigue.

evolution of the probability vector with the fatigue damage. At this stage, the information on damage is enhanced compared to what was available in the earlier cycles. At the onset of the crack propagation phase, the histograms of probability distribution show drastic changes in patterns, which indicate rapid development of large cracks.

The image in each of Figs. 6(e), 7(e), 8(e) and 9(e) exhibits a fully developed crack in its propagation phase. The corresponding bottom plate shows the histogram of the probability distribution that is significantly different from those in earlier cycles in plate pairs (a)–(d), which shows further gain in the information on crack damage. The image in each of Figs. 6(f) and 7(f) exhibits a completely broken specimen at ~80 kilocycles for low-cycle fatigue. Similarly, the image in each of Figs. 8(f) and 9(f) exhibits a completely broken specimen at ~240 kilocycles for high-cycle fatigue. The corresponding bottom plates show the delta distribution indicating complete information on crack damage.

The observation in Figs. 6–9 is further clarified by using the notion of entropy (see Eq. (2)). The data at the nominal condition have been partitioned using the maximum entropy principle, which leads to uniform probability distribution as seen in the bottom plate of plate pair (a) in Figs. 6–9. In contrast, for the completely broken stage of the specimen, the entire probability distribution is concentrated in only one state as seen in the bottom plate of plate pair (f) in Figs 6–9, due to very large attenuation of the ultrasonic signal. This phenomenon of the test specimen being completely broken signifies certainty of information and hence zero entropy. Therefore, as the fatigue crack damage evolves, the uniform distribution (i.e., maximum entropy) under nominal condition degenerates toward the delta distribution (i.e., zero entropy) for the broken specimen. In the intermediate stages, gradual degradation can be quantitatively evaluated using this information.

Fig. 10 shows the evolution of anomaly measure profiles obtained by STSA of ultrasonic data for low-cycle and high-cycle fatigue and the corresponding crack growth plots. The top plate on the left column in Fig. 10 shows profiles of anomaly measure for both left and right sides of the notch under low-cycle fatigue. Similarly, the top plate on the right column shows profiles of anomaly measure for both left and right sides of the notch under high-cycle fatigue. The bottom plates show the corresponding crack growth profiles. In each curve in the top plates of Fig. 10, the sharp change in the slope of the anomaly measure indicates the onset of crack propagation phase. This

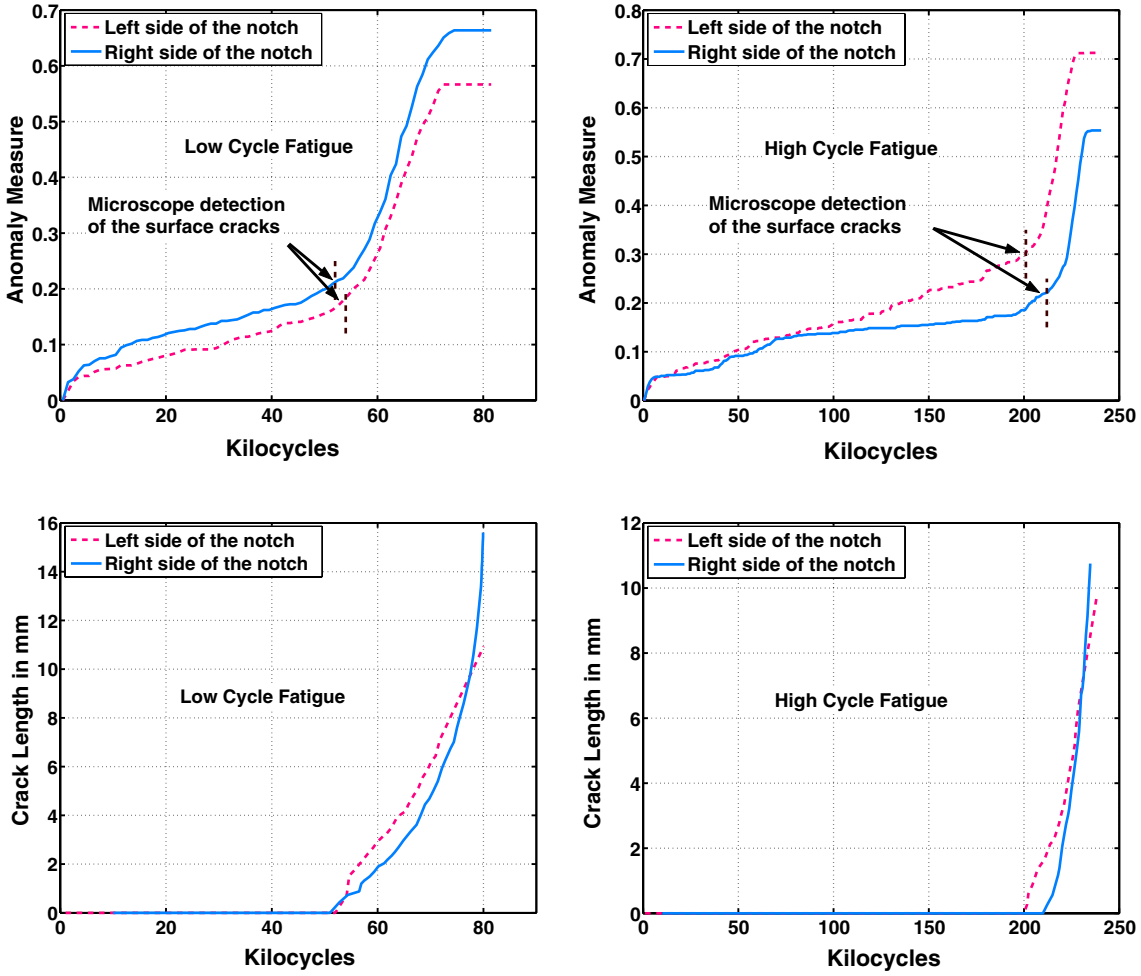

Fig. 10. Profiles of anomaly measure and crack growth for center-notched specimens under low cycle and high-cycle fatigue.

occurs approximately upon appearance of a surface crack. The vertical dashed lines in the top two plates of Fig. 10 indicate the first detection of a surface crack by the optical microscope.

It is observed that small changes can be detected by STSA significantly before the microscope can capture a surface crack. The slope of the anomaly measure represents the fatigue damage growth rate while the magnitude indicates the accumulated fatigue damage starting from the nominal condition. An abrupt increase in the slope (i.e., a sharp rise in the curvature) of anomaly measure profile provides a clear insight into a forthcoming failure. The region to the right of the vertical dashed lines for left side and right side anomaly measure curves in the top plate on left column of Fig. 10 can be considered to be the boundary of the crack initiation and crack propagation phases, where the growth of anomaly measure is significantly faster than that in the crack initiation phase. However, the critical information lies in the region towards the left of the vertical lines which is broadly identified as crack initiation phase where no crack was visible on the surface. This is the region where micro-structural damage such as multiple small cracks possibly caused small changes in the ultrasonic signal profile. After the multiple small cracks coalesce together to form a single large crack, the crack propagation phase starts. Damage evolution undergoes elastoplastic deformation under low-cycle fatigue due to a large number of dislocation movements and multiple small cracks develop from a very early stage. Similar effects are observed for high-cycle fatigue as seen in the top plate on right column of Fig. 10. In the region towards the right of the vertical dashed lines, anomaly measure profiles show significantly faster growth as compared to the slow growth during crack initiation towards the left of the vertical lines. For low-cycle fatigue, a relatively large slope in the anomaly measure is observed even during crack initiation region indicating occurrence of significant damage during this phase. Crack initiation prevailed for ~52–55 kilocycles for low-cycle fatigue, which is ~68% of the total life. For high-cycle fatigue, crack initiation prevailed for a relatively longer period of ~205–215 kilocycles for development of a single large crack, which amounts to ~87% of the total life.

The top two plates in Fig. 10 show a relatively large slope of anomaly measure from the start of cyclic loading to ~5 kilocycles for both low-cycle and high-cycle fatigue.

This is the stage where micro-structural damage (e.g., due to dislocation movements and accumulation, and persistent slip band formation) induces hardening of the strained components [45] and changes the ultrasonic impedance leading to a sharp rise in the local slope of the anomaly measure profile. After these initial effects subside, a modest reduction of the slope takes place for the remaining part of the crack initiation phase. A sharp rise of slope is again observed at the onset of the crack propagation phase. Similar phenomena were observed by Berkovits and Fang [47] in acoustic emission experiments on smooth specimens of Incoloy 901 at room temperature. Further experiments and micro-structural analysis are necessary to confirm these findings.

7. Summary, conclusions, and future work

This paper presents the concept, theory, and experimental validation of a statistical pattern identification tool for early detection and online monitoring of fatigue damage in polycrystalline alloys. The underlying principle of fatigue damage detection is built upon symbolic time series analysis of ultrasonic sensor signals. A combination of maximum-entropy partitioning in the wavelet domain and symbolic dynamics enables fatigue damage detection significantly before the onset of crack propagation. The codes of damage analysis are executable in real time and have been demonstrated on a special-purpose fatigue testing apparatus on 7075-T6 aluminum alloy specimens under: stress controlled low-cycle fatigue and stress controlled high-cycle fatigue. The results consistently indicate that the code is capable of detecting damage before any surface cracks are captured by the optical microscope.

The reported work is a step toward building a reliable instrumentation system for early detection of fatigue damage in polycrystalline alloys. Further experimental, analytical and micro-structural research is necessary before its usage in industry. While there are many technical issues that need to be addressed, the following research topics are being currently pursued.

- Statistical analysis of an ensemble of ultrasonic time series data sets, collected under identical loading and environmental conditions, to account for manufacturing and material uncertainties.
- Microstructural analysis to investigate the early stages of fatigue damage.
- Validation of the STSA technique for fatigue damage monitoring under different conditions, such as variable-amplitude block loading and spectral loading.

References

[1] Ozekici S. Reliability and maintenance of complex systems, vol. 154, NATO Advanced Science Institutes (ASI) Series F: Computer and Systems Sciences, Berlin, Germany, 1996.
[2] Meggiolaro M, Castro J. Statistical evaluation of strain-life fatigue crack initiation predictions. Int J Fatigue 2004;26:463–76.
[3] Ishihara S, McEvily A. Analysis of short fatigue crack growth in cast aluminium alloys. Int J Fatigue 2002;24:1169–74.
[4] Bjerkén C, Melin S. A tool to model short crack fatigue growth using a discrete dislocation formulation. Int J Fatigue 2003;25:559–66.
[5] Ramsamooj D. Analytical prediction of short to long fatigue crack growth rate using small- and large-scale yielding fracture mechanics. Int J Fatigue 2003;25:923–33.
[6] Pathria R. Statistical mechanics. Elsevier Science and Technology Books; 1996.
[7] Sobczyk K, Spencer B. Random fatigue: Data to theory. Boston, MA: Academic Press; 1992.
[8] Ott E. Chaos in dynamical systems. Cambridge University Press; 1993.
[9] Keller E, Ray A. Real time health monitoring of mechanical structures. Struct Health Monitor 2003;2(3):191–203.
[10] Grondel S, Delebarre C, Assaad J, Dupuis J, Reithler L. Fatigue crack monitoring of riveted aluminium strap joints by lamb wave analysis and acoustic emission measurement techniques. NDT & E Int 2002;35:137–46.
[11] Cook D, Berthelot Y. Detection of small surface-breaking fatigue cracks in steel using scattering of rayleigh waves. NDT & E Int 2001;34:483–92.
[12] Zilberstein V, Walrath K, Grundy D, Schlicker D, Goldfine N, Abramovici E, et al. Mwm eddy-current arrays for crack initiation and growth monitoring. Int J Fatigue 2003;25:1147–55.
[13] Witney A, Li YF, Wang J, Wang MZ, DeLuccia JJ, Laird C. Electrochemical fatigue sensor response to Ti-6 wt.% Al-4 wt.% v and 4130 steel. Philos Mag 2004;84(3–5):331–49.
[14] Yang B, Liaw PK, Wang G, Peter WH, Buchanan R, Yokoyama Y, et al. Thermal-imaging technologies for detecting damage during high-cycle fatigue. Metall Mater Trans A 2004;35A:15–24.
[15] Baram J. Fatigue-life prediction by an order statistics treatment of acoustic-emission signals. Exp Mech 1993;33:189–94.
[16] Harris DO, Dunegan HL. Continuous monitoring of fatigue–crack growth by acoustic-emission techniques. Exp Mech 1974;14:71–80.
[17] Lee KY. Cyclic ae count rate and crack growth rate under low cycle fatigue fracture loading. Eng Fracture Mech 1989;34(5/6):1069–73.
[18] Lysak MV. Development of the theory of acoustic emission by propagating cracks in terms of fracture mechanics. Eng Fracture Mech 1996;55(3):443–52.
[19] Scala M, Cousland SM. Acoustic emission during fatigue crack propagation in the aluminium alloys 2024 and 2124. Mater Sci Eng 1983;61:211–8.
[20] Zilberstein V, Grundy D, Weiss V, Goldfine N, Abramovici E, Newman J, et al. Early detection and monitoring of fatigue in high strength steels with mwm-arrays. Int J Fatigue 2005;27:1644–52.
[21] Bai HS, Yu LY, He (Ho) JW. A monitoring system for contact fatigue crack testing. NDT Int 1989;22(3):162–7.
[22] Yusa N, Janousek L, Rebican M, Chen Z, Miya K, Chigusa N, et al. Detection of embedded fatigue cracks in inconel weld overlay and the evaluation of the minimum thickness of the weld overlay using eddy current testing. Nucl Eng Des 2006;236(18):1852–9.
[23] Anson L, Chivers R, Puttick K. On the feasibility of detecting pre-cracking fatigue damage in metal matrix composites by ultrasonic techniques. Compos Sci Technol 1995;55:63–73.
[24] Vanlanduit S, Guillaume P, Linden G. Online monitoring of fatigue cracks using ultrasonic surface waves. NDT & E Int 2003;36:601–7.
[25] Rokhlin S, Kim JY. In situ ultrasonic monitoring of surface fatigue crack initiation and growth from surface cavity. Int J Fatigue 2003;25:41–9.
[26] Kenderian S, Berndt T, Green R, Djordjevic B. Ultrasonic monitoring of dislocations during fatigue of pearlitic rail steel. Mater Sci Eng 2003;348:90–9.
[27] Daw C, Finney C, Tracy E. A review of symbolic analysis of experimental data. Rev Sci Instrum 2003;74(2):915–30.
[28] Ray A. Symbolic dynamic analysis of complex systems for anomaly detection. Signal Process 2004;84(7):1115–30.

[29] Chin S, Ray A, Rajagopalan V. Symbolic time series analysis for anomaly detection: A comparative evaluation. Signal Process 2005;85(9):1859–68.
[30] Gupta S, Ray A, Keller E. Symbolic time series analysis of ultrasonic data for early detection of fatigue damage. Mech Syst Signal Process. Available from: www.ScienceDirect.com, in press.
[31] Rajagopalan V, Ray A. Symbolic time series analysis via wavelet-based partitioning. Signal Process 2006;86(1):3309–20.
[32] Lind D, Marcus M. An introduction to symbolic dynamics and coding. United Kingdom: Cambridge University Press; 1995.
[33] Badii R, Politi A. Complexity hierarchical structures and scaling in physics. United Kingdom: Cambridge University Press; 1997.
[34] Hopcroft H, Motwani R, Ullman J. Introduction to automata theory, languages, and computation. 2nd ed. Boston: Addison Wesley; 2001.
[35] Abarbanel H. The analysis of observed chaotic data. New York: Springer-Verlag; 1996.
[36] Davidchack R, Lai Y, Bolt E, Dhamala H. Estimating generating partitions of chaotic systems by unstable periodic orbits. Phys Rev E 2000;61:1353–6.
[37] Kennel M, Buhl M. Estimating good discrete partitions form observed data: Symbolic false nearest neighbors. Phys Rev E 2003;91(8):084–102.
[38] Mallat S. A wavelet tour of signal processing 2/e. Academic Press; 1998.
[39] Cover TM, Thomas JA. Elements of information theory. New York: John Wiley; 1991.
[40] Naylor AW, Sell GR. Linear operator theory in engineering and science. New York: Springer-Verlag; 1982.
[41] Keller EE, Real time sensing of fatigue crack damage for information-based decision and control. PhD thesis, 2001, Department of Mechanical Engineering, Pennsylvania State University, State College, PA.
[42] Nagy P. Fatigue damage assessment by nonlinear ultrasonic materials characterization. Ultrasonics 1998;36:375–81.
[43] Cantrell J, Yost W. Nonlinear ultrasonic characterization of fatigue microstructures. Int J Fatigue 2001;23:487–90.
[44] Rose J. Ultrasonic waves in solid media. Cambridge University Press; 2004.
[45] Suresh S. Fatigue of materials. Cambridge, UK: Cambridge University Press; 1998.
[46] Toolbox Wavelets, MATLAB. Mathworks Inc.
[47] Berkovits A, Fang D. Study of fatigue crack characteristics by acoustic emission. Eng Fracture Mech 1995;51(3):401–16.